Biophysical Journal
Article

Biophysical Society

Pinching and pushing: fold formation in the *Drosophila* dorsal epidermis

Vijay Velagala[1,2] and Jeremiah J. Zartman Ph.D.[1,2,*]
[1]Department of Chemical and Biomolecular Engineering and [2]Bioengineering Graduate Program, University of Notre Dame, Notre Dame, Indiana

ABSTRACT Epithelial folding is a fundamental morphogenetic process that shapes planar epithelial sheets into complex three-dimensional structures. Multiple mechanisms can generate epithelial folds, including apical constriction, which acts locally at the cellular level, differential growth on the tissue scale, or buckling because of compression from neighboring tissues. Here, we investigate the formation of dorsally located epithelial folds at segment boundaries during the late stages of *Drosophila* embryogenesis. We found that the fold formation at the segment boundaries occurs through the juxtaposition of two key morphogenetic processes: local apical constriction and tissue-level compressive forces from posterior segments. Further, we found that epidermal spreading and fold formation are accompanied by spatiotemporal pulses of Hedgehog (Hh) signaling. A computational model that incorporates the local forces generated from the differential tensions of the apical, basal, and lateral sides of the cell and active forces generated within the whole tissue recapitulates the overall fold formation process in wild-type and Hh overexpression conditions. In sum, this work demonstrates how epithelial folding depends on multiple, separable physical mechanisms to generate the final morphology of the dorsal epidermis. This work illustrates the modularity of morphogenetic unit operations that occur during epithelial morphogenesis.

SIGNIFICANCE Head involution occurs in two phases, with epithelial folds forming at the segment boundaries after the dorsal epidermis reaches the anteriormost region of the embryo during the final stages of *Drosophila* embryogenesis. Spatiotemporal pulses of Hh signaling are observed during head involution and fold formation. Fold formation at segment boundaries occurs because of a combination of two morphogenetic operations: apical constriction and contractile forces driving the tissue movement. Disruption of patterned Hh activity inhibits apical constriction but not tissue movement, leading to incomplete folding. A computational model recapitulates tissue folding phenotypes observed in wild-type and Hh signaling perturbation cases.

INTRODUCTION

The morphogenesis of animal organs depends on intricate and dynamic cellular processes driven by genetic programs, guided by microenvironmental cues, and coordinated through intercellular communication (1,2). During development, gene expression patterns regulate cell mechanics and cell shape to build tissues. Examples of morphogenetic modules include epithelial spreading and folding (1,3,4). Both processes are used to transform two-dimensional epithelial sheets into three-dimensional structures. Controlled epithelial spreading and folding occur throughout development from gastrulation to organogenesis. Their dysregulation leads to diseases such as congenital disabilities and cancer. However, how these coordinated cell shape changes are regulated by global patterning information during epithelial morphogenesis remains poorly understood. A better understanding of how the biophysical properties of cells are regulated is needed to more effectively repair defects during embryonic development (5), wound healing (6), and the diagnosis and treatment of metastatic tumors (7).

In particular, epithelial folding is ubiquitous throughout development and essential for the formation of different organs, such as neural tubes (8), villi (9), crypts (10), etc. The robustness of these shapes is achieved through simple biophysical mechanisms (4). Forces behind these mechanisms can occur within few cells or throughout the whole tissue. One widely studied mechanism is apical constriction, in which cells apically reduce their area while maintaining

Submitted July 10, 2021, and accepted for publication August 24, 2021.
*Correspondence: jzartman@nd.edu
Editor: Stanislav Shvartsman.
https://doi.org/10.1016/j.bpj.2021.08.028

constant volumes (11–13). Besides apical constriction, other mechanisms such as the basal shift of adherens junctions (14) and increase in lateral tension (15) act as a driver of epithelial folding. In the above-mentioned scenarios, the folding cells generate the forces, which act locally to drive the fold formation. In addition to local active forces, forces from the tissue neighboring to the folding cells can also contribute to folding (3). For example, salivary gland invagination in *Drosophila* embryos occurs even after the loss of apical constriction (16). In this case, the tissue-level myosin cable generates compressive force, which drives the salivary gland invagination. Hence, the forces driving the fold formation can vary from a few cells to a whole tissue, depending upon the developmental context. Here, we investigate a similar phenomenon in a poorly characterized stage of development, in which the forces within a segment of the *Drosophila* epidermis drive fold formation at the segment boundaries at the end of head involution (Fig. 1, *A* and *B*).

During the later stages of embryogenesis, the dorsal epidermis moves over the head tissue in the anterior direction, whereas the head tissue slides under the epithelia in the posterior direction (18). This process, known as head

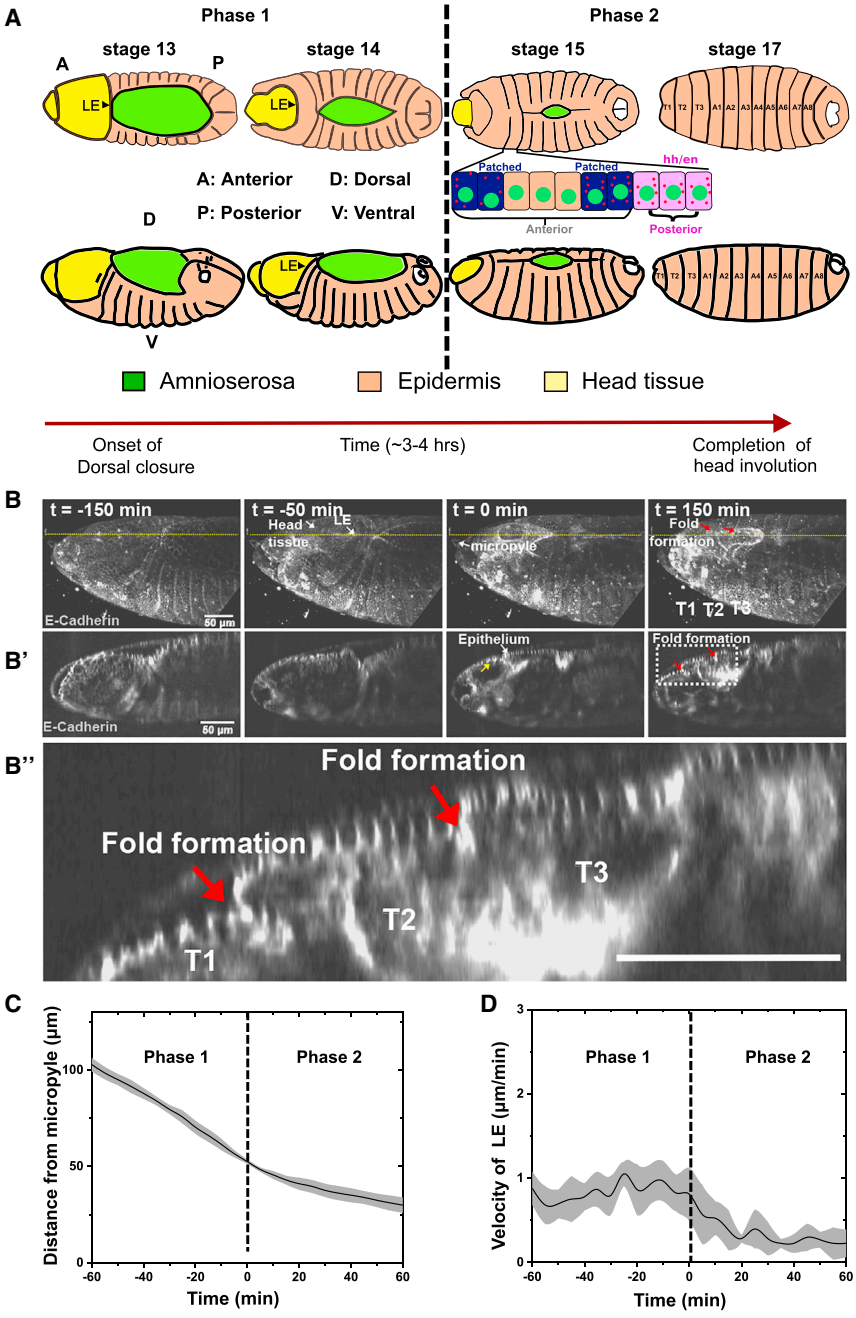

FIGURE 1 The late stages of epidermal morphogenesis include epithelial spreading during head involution and fold formation. (*A*) Schematic of head involution; top (dorsal view); bottom (lateral view). (*B*) Time-lapse images of epithelial spreading and fold formation in a *Drosophila* embryo expressing *E-cadherin: GFP*. (*B'*) Cross-sectional view. Here, the time t = 0 is taken as the time when the leading edge (LE) is 50 μm from the micropyle, following the nomenclature of (17). (*B'*) Cross-sectional view of the embryo during spreading and fold formation. (*B''*) Enlarged view of the folds (scale bars, 50 microns). (*C*) Graph showing the distance of the LE from the micropyle with respect to time. (*D*) Graph showing the velocity of the LE with respect to time during *Drosophila* head involution. Based on the velocity profile, epithelial spreading can be divided into two phases (n = 5 embryos). In phase 1, the velocity is constant and higher than the phase 2 velocity. To see the figure in color, go online.

involution, is required for internalizing the head tissue. Once the LE of the dorsal epithelium reaches the anterior end of the embryo, the whole epithelium starts to form folds at precise locations known as segment boundaries, such as at the T1-T2 boundary (Fig 1, *A* and *B*) . These folds act as a boundary between the segments of the epithelia and are important for segmenting the epidermis. After the initial patterning early in embryogenesis, the segment polarity genes maintain their expression pattern in each segment and divide each segment into anterior and posterior compartments. Expression of these segment polarity genes are known to provide the precise spatial information for the formation of grooves at parasegment and segment boundaries during stages 10 and 12–13 of embryogenesis (19–21). For example, a recent study shows that Wingless signaling acts downstream to suppress folding at the parasegment boundaries (20), whereas Hh is necessary for inducing groove cell fate at the segment boundaries (19). Hence, the maintenance and expression of these segment polarity genes are essential for cells to form grooves or folds at precise locations.

Hh signaling is one of the key biochemical pathways that regulate several fundamental processes (22), including cell growth, differentiation, polarity (23), and apoptosis (24). Hh signaling is vital for key developmental aspects in both fruit flies and vertebrates (25). Aberrations in Hh signaling leads to a diverse range of human cancers, such as brain, lung, pancreas, and prostate cancers (26). Hence, the activity of Hh signaling is required to be precisely controlled to avoid morphogenetic defects (27). Some questions regarding Hh signaling include how the gradients of Hh signaling are generated and maintained during epithelial morphogenesis (28). Also, questions about how the developmental outcome depends on the duration and strength of signaling remain incompletely answered (29), and whether these gradients are static or dynamic later in development needs to be investigated.

In *Drosophila*, Hh protein is released by the posterior cells of each segment, and it diffuses to the adjacent anterior compartments. In the anterior compartment, Hh binds to its receptor Patched (Ptc) and activates the downstream transcription factor Cubitus interruptus (Ci) (22). Once Hh binds to Ptc, the transducer Smoothened is released from Ptc inhibition and gets localized to the cell surface (30,31). When Smoothened is localized to the cell surface, it stabilizes the downstream transcription factor Ci by converting it into transcriptional active Ci^{A} form to replace the transcriptional repressor Ci^{R} (31–33). The transcriptional activator further activates the downstream target genes. In the posterior compartment, Ci transcription is repressed by Engrailed. Therefore, even though the posterior compartment cells express Hh, they cannot transduce Hh signaling (34). In summary, Hh is secreted in the posterior compartment, and signaling is activated in the adjacent anterior compartments.

Here, our study uncovers new facets in the late stages of *Drosophila* embryogenesis, when much less is known about morphogenesis. We discovered that there are spatiotemporal pulses of Hh signaling during head involution and fold formation at segment boundaries. Our study shows that the formation of folds at the segment boundaries is initiated by cells undergoing apical constriction at the segment boundaries (35), followed by contractile forces from the posterior segments driving the T2 segment over constricted cells. Further, this study shows that the Hh signal is temporally patterned during this process and that disruption of the pattern by uniform overexpression in the dorsal epidermis prevents apical constriction at the segment boundaries. However, the forces from the actomyosin contractile rings, which form because of the relative alignment of cell bonds along the dorsal-ventral (D-V) axis (Fig. S2) within the T2 segment, drive the tissue movement, exerting compressive stress on the cells in the T1 and T2 segments, leading to the formation of ectopic boundaries. Computational models describing the biophysics of morphogenesis combined with experimental results are necessary for uncovering the mechanisms behind morphogenesis and often provide new insights (36–41). So we implemented a mechanical model representing the cross section of the T1-T2 segment. This computational model recapitulates the final tissue morphology as seen experimentally when both constriction and contractile forces are incorporated. The model shows that the apical constriction is necessary for proper fold formation, in which tangential forces alone are only sufficient to form ectopic boundaries characterized by local wrinkling. Altogether, these results suggest a mechanism for the formation of the fold at the T1-T2 segment boundary, where both cellular-level forces and tissue-level forces drive the folding process.

MATERIALS AND METHODS

Embryo collection and live imaging

All crosses were set up at 25°C in a fly cage attached to a grape juice agar plate. Embryos were collected on agar plates after 12 h. Embryos collected from the agar plates were dechorionated using 50% bleach and washed thoroughly. After washing, embryos were mounted on the dorsal side in a circular well of a petri dish. Halocarbon oil (catalog number (#) H8898; Sigma-Aldrich, St. Louis, MO) was used as the mounting medium to mount the embryos. Mounted embryos were imaged using Nikon Eclipse Ti confocal microscope with a Yokogawa spinning disk (Tokyo, Japan) at 40× (air objective, NA 0.60), 40× (oil objective, NA 1.30), 60× (oil objective, NA 1.49), and 100× (oil objective, NA 1.49), depending upon the experiment. Images were collected at 5- or 15-min time intervals.

Drosophila genetics and strains

Drosophila stocks were grown on standard laboratory cornmeal food. The following stocks were used for the experiment: *pannier*-GAL4 driver (*pnr-Gal4*), *moesin: GFP* (Bloomington (BL) #58788), *UAS-hh* (Kornberg laboratory), cholesterol-free Hh *UAS-hh.N.GFP* (42) (BL #81023), *Hh::GFP* (43) (BL #86271), *Ptc::mcherry* (43) (BL #86272), *E-cadherin::GFP; pnr-Gal4 squash::mcherry* (44) (Yanlan Mao's laboratory).

Fluorescent immunostaining

Embryos were collected after 12 h and dechorionated using 50% bleach. Dechorionated embryos were fixed in 4% paraformaldehyde (#22050133; Thermo Fisher Scientific, Waltham, MA) and further blocked using 5% Normal Goat Serum (#NC9660079; Jackson ImmunoResearch Laboratories, West Grove, PA). After blocking, embryos were washed overnight with primary antibodies and then washed with 0.02% PBT (Phosphate-buffered saline with Triton). After incubation of the primary antibodies, embryos were washed with the corresponding secondary antibodies and then washed with PBT. After primary and secondary washes, embryos were mounted on a coverslip using Vectashield (H-1000; Vector Laboratories, Burlingame, CA).

Image processing and analysis

All images were processed using FIJI (45). TIFF (Tag Image File Format) stacks generated from the experiments were opened using FIJI, and the background was subtracted using a rolling ball. After background subtraction, deconvolution was performed for Fig. 2 *A* and Fig. 3 *A* using CSBDEEP (46). Deconvoluted stacks were projected using maximal intensity. Maximal intensity projection images were exported to Epyseg (47) for segmenting cells. Cell shapes are quantified using a written Matlab code (The MathWorks, Natick, MA) or manually using FIJI (45).

Light-sheet imaging

Light-sheet imaging was performed using a Luxendo MUVI-SPIM microscope (Bruker, Billerica, MA) equipped with 16× (NA 0.8) water immersion objective lenses and scientific complementary metal-oxide-semiconductor Orca Flash4.0 V3 cameras (Hamamatsu Photonics, Hamamatsu City, Japan). Samples were imaged at 32× magnification using a 2× magnification changer. Dechorionated embryos were loaded into 100 μL micropipettes (Blaubrand, Wertheim, Germany) using 0.8% agarose/phosphate-buffered saline. Images from the opposing detection objectives were fused using LuxControl software (version 3.4.0; Bruker), and image processing was performed using FIJI (Video S1) and Imaris (Video S4).

Computational modeling

A computational model of the T1/T2 segment fold was implemented using Surface Evolver (48), which calculates the surface energy of the system and minimizes it using a gradient descent method. In this model, an initial configuration of the cross section of the T1-T2 segment was generated by creating a one-dimensional row of cells with apical, lateral, and basal surfaces. We assumed that the volume of the cells remained constant. Apical, basal, and lateral edges are one-dimensional representations of their

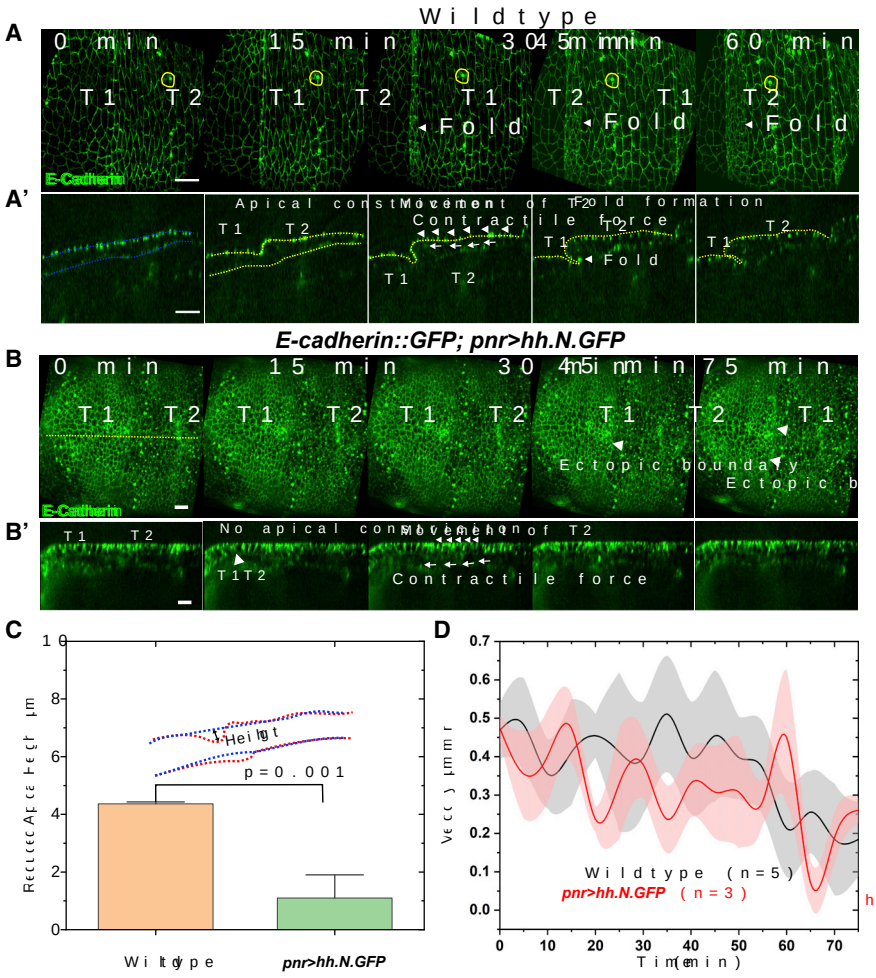

FIGURE 2 Epithelial folding at T1/T2 segment boundary is due to a combination of apical constriction at the segment boundary and movement of the segment. (*A*) Time-lapse images showing the epithelial folding in the dorsal epidermis during later stages of *Drosophila* embryogenesis. Here, t = 0 is the time when the LE reaches the anterior end of the embryo and fold formation begins. White arrow indicates the folds. Deconvolution was performed using CSBdeep. (*A'*) Cross-sectional view of the dorsal epidermis showing the epithelial folding in a wild-type embryo. Initially, the apical height of the cells is reduced at the segment boundary. Then, the forces within T2 segment drive the tissue forward, resulting in the movement of T2 over apically constricted cells. (*B*) Uniform activation of the Hh pathway blocks epithelial fold formation at segment boundaries. Time-lapse images showing *Drosophila* embryos with uniform overexpression of cholesterol-free Hh in the dorsal epidermis. Overexpression of Hh in the dorsal epidermis leads to the loss of epithelial folds. The white pointer indicates the absence of epithelial folds and the formation of ectopic boundary. (*B'*) Time-lapse images showing the cross-sectional views of the epithelial folding in *Drosophila* embryo with uniform overexpression of cholesterol-free Hh. Loss of apical constriction at the segment boundary can be viewed. However, the presence of contractile forces drive the movement of the segment, resulting in the formation of ectopic boundaries. (*C*) Graph comparing the reduction in the apical height of the cells at the T1-T2 segment boundary during fold formation for both wild-type and Hh overexpression. (*D*) Graph comparing the velocity of the T2 segment during fold; the velocity is calculated by tracking an E-cadherin cluster located at the center of the T2 segment. All scale bars represent 10 microns. To see the figure in color, go online.

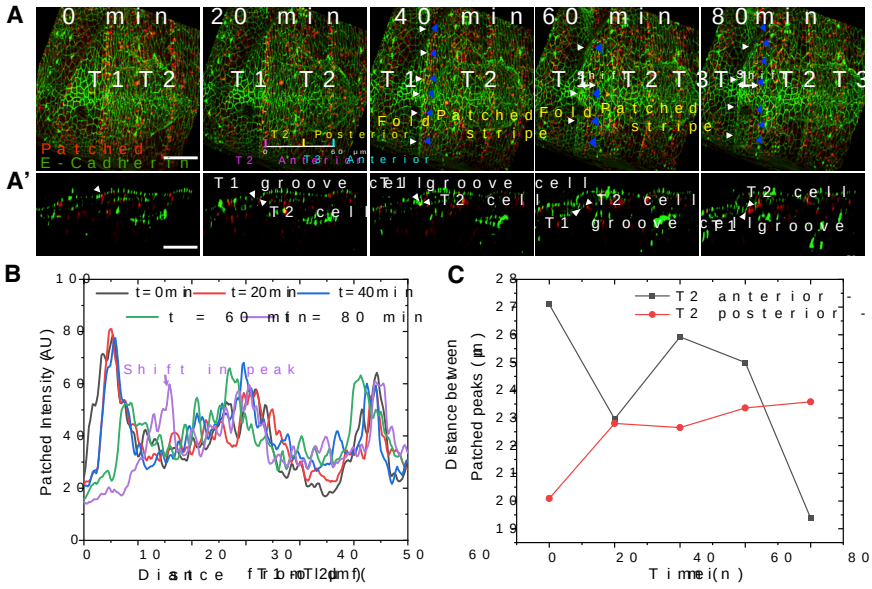

FIGURE 3 Ptc dynamics confirm apical constriction occurs at the T1-T2 segment boundary. (*A*) Time-lapse images showing the Ptc dynamics in an embryo expressing *E-cadherin::GFP* and *Ptc:: mcherry*. As shown, the Ptc peak (*blue arrow*) shifts away from the fold (*white arrow*), indicating that the T2 segment moves over the folded cells. Here, t = 0 is the time when the LE completed its movement, and the folds begin to form. (*A'*) Time-lapse images showing the cross-sectional view in which cells T1 and T2 located at the segment boundary, undergo constriction. White arrows indicate the groove cell and T2 cell expressing Ptc receptor, which is located adjacent to the groove cell on the posterior side. Cross-sectional view confirms that the deepest groove cell does not express Ptc. (*B*) Quantification of Ptc dynamics during the folding reveals that the anterior peak has higher intensity when compared with the posterior. During the fold formation, the peak moves away from the fold boundary, confirming that the T2 segment overlaps and moves over the anterior end. (*C*) Graph showing the distance between two adjacent peaks of a Ptc stripe. Distance between the T2-anterior and T2-posterior peaks decreases as the folding progresses, whereas the distance between the T2-posterior and T3-anterior remains the same. The resulting shift is due to the fold formation as the T2 segment moves over its anterior part, resulting in the reduction in the distance between two peaks. All scale bars represent 25 microns. To see the figure in color, go online.

surfaces. The total energy of the system is equivalent to the total surface energy of the system, which is denoted by (49,50)

$$w = \alpha l_a + \beta l_b + l_l$$

where l_a, l_b, and l_l represent the reduced, nondimensionalized apical, basal, and lateral lengths, and α and β denote the ratio of apical and basal to lateral tension, respectively. Further, we incorporated the effect of contractile forces in the model by applying an external horizontal force on the cells in the T2 segment. For every time step, the external force moves the T2 segment, followed by the calculation of net forces on the cell vertices and displacement of vertices using equations of motion (51,52). The total simulation was run for around 1200 time steps, which in real time corresponds to an approximate developmental time of 2–3 h.

RESULTS

Epithelial fold formation occurs at segmental boundaries after head involution

During *Drosophila* head involution, the epithelial LE progresses toward the anterior end of the embryo (17) (Fig. 1, *A* and *B*), whereas the head tissue simultaneously slides under the epithelia in the posterior direction. Tracking the movement of the LE reveals that the spreading can be divided into two phases characterized by the velocity profiles (Fig. 1 *D*). During phase 1, the LE moves at a velocity of ~1 μm/min, which initiates concurrently while dorsal closure proceeds (18,53,54). During this process, the epithelial cells expand their widths along the anterior-posterior axis. During phase 2, when LE reaches a position of at least 50 μm from the anterior end of the head tissue, the velocity of the LE shows a decreasing trend. Once the LE reaches the anterior end of the embryo at ~50 min (Fig. 1 *B*), the epithelial sheet folds at the segment boundaries. An initial fold is formed between the T1 and T2 segments, and subsequently, a fold is formed at the T2 and T3 segment boundaries (Fig. 1 *B*; Video S1). Czerniak et al. (17) proposed that the initial movement of the dorsal epithelium is due to the tangential forces (hoop stresses) generated by the gradient of normal tension exerted by the actomyosin cables around the embryo. Once the T1 segment reaches its final position, the tangential force within the T2 segment drives its movement. Because of the motion of the T2 segment, and T1 segment being stationary at this time point, the anterior end of T2 segment folds over the T1 segment and overlaps with the T1 segment.

To further clarify the mechanism behind the fold formation, we looked at the cross-sectional view of the dorsal epithelia during this process. We observed that once the LE reaches the anterior end, the intersegmental groove formation begins (Video S2). During the segmental groove formation, the cells located at the T1-T2 segment boundary reduce their apical heights and move toward the interior of the embryo (Fig. 2, *A*, *A'*, and *C*). As it moves toward the interior of the embryo, it pulls along the neighboring cells. The cells located at the bottom of the groove are known as groove cells, whereas the cells adjacent to them are known as groove founder cells (21). As mentioned earlier, contractile forces present in the segment drive the movement of the T2 segment cells over the segmental groove. To quantify the movement of the T2 segment, we tracked the movement of the T2 segment during this process and measured its velocity. From the velocity profile, we

observed that the segment moves at a velocity of around 0.5 μm/min (Fig. 2 *D*). As the T2 segment moves over the segmental groove, the anterior end of the T2 segment overlaps the T1 segment, resulting in a fold. As the fold progresses, we observe a similar mechanism in which the groove begins to form at the T2-T3 segment boundary, followed by the movement of the T3 segment over the T2 segment. Together, our results propose that groove formation at the segment boundaries initiates the fold formation, whereas the forces within the T2 and T3 segment drive the motion of the segment over the groove (Video S2).

Larsen et al. (21) showed that the Hh signaling is required for the groove formation, and the most posterior cell of the preceding segment (T1) apically constricts and also lies at the bottom of the groove. To confirm whether we observe a similar behavior during late stages of embryogenesis, we studied the dynamics of Hh receptor Ptc along with a cell membrane marker. Our study confirms that the cells expressing Ptc are located adjacent to the posterior cells, resulting in two stripes of Ptc-expressing cells in each segment (Video S3). Quantification of the intensity profiles reveals that the anterior stripe has a steeper gradient when compared to the posterior stripe (Fig. 3 *B*). When we looked at the cross-sectional views of the dorsal epithelia along with the Ptc receptor during folding, we observed that the cell that undergoes constriction and is located at the bottom of the groove does not express Ptc. However, the cell located just adjacent to posterior side of the groove cell does have Ptc expression, confirming that the most posterior cell of the preceding segment forms the bottom of the groove (Fig. 3, *A* and *A'*). This result confirms that the cells from both the T1 and T2 segments participate in the groove formation, whereas the forces within the T2 segment drive the movement of the T2 over the groove and groove founder cells.

Pulses of Hh signaling precedes head involution and epithelial spreading

Previously, Hh signaling was shown to regulate groove cell specification (19). Therefore, we asked whether the gradient is relatively static or if the dynamics of Hh signaling play any role during head involution and fold formation. To monitor Hh activity, we used the Hh: GFP fly line, which is expressed at physiological levels using a bacterial artificial chromosome transgene construct (43) (Fig. 4 *A*). As expected, we observed that Hh expression dynamics are confined to the posterior compartments. Surprisingly, we observed a broader band of Hh expression posterior to the LE during the initial stages of epithelial spreading. This Hh expression that is juxtaposed to the LE decreases as the epidermis continues to spread during phase 2 (Fig. 4 *B*; Video S4). Of interest, the decline in Hh expression coincides with the velocity decrease that occurs during phase 2 (Fig. 4 *C*). Moreover, we observed that the intensity of Hh signaling in each segment increases to a maximum and then decreases during head involution and fold formation (Video S4). Further, we also observed that there is a short-range activity of Hh signaling in the head tissue during the head involution. However, we did not observe any interesting changes in the signaling activity during fold formation. In addition, light-sheet imaging of the embryo revealed that the movement of the ventral epidermis initiates the head involution (Video S4). Moreover, we observed that the Hh signaling is active in a stripe of cells located in the center of the head tissue during head involution (Fig. S4). Together, these results suggest that the Hh signaling dynamics are spatiotemporally patterned during *Drosophila* head involution and fold formation.

Uniform activation of Hh signaling inhibits fold formation but not tissue compression

Next, we investigated the significance of patterned Hh signaling during fold formation. To do so, we uniformly overexpressed Hh in the dorsal epidermis. Previous studies show that Hh overexpression in the dorsal epidermis resulted in a slower movement of epithelia and altered segment positioning by homogenizing the patterned contractile forces (17). Mulinari et al. showed that Hh signaling induces groove fate to cells at the segment boundary in the dorso-lateral epidermis, and uniform activation of Hh induces groove fate to all cells (19). Thus, we asked whether the uniform expression of Hh signaling influences fold formation. We uniformly expressed Hh in the dorsal epidermis using the *pnr-Gal4* (55), as *pannier* is expressed only in the dorsal epidermis and expressed only during later stages of embryonic development. Interestingly, overexpression of Hh in the dorsal epidermis arrested the movement of the LE (Fig. 4 *D*; Video S5; (17)). In contrast to a previous report, which shows that uniform overexpression of Hh completes the head involution, we found cases in which the epithelial movement halted, leading to incomplete head involution. Next, we tested whether uniform overexpression of Hh signaling has any effect on the fold formation at segment boundaries (Fig. 2 *B*). We observed that the groove formation was not observed at the segment boundaries. We found a similar phenomenon with the expression of a cholesterol-free Hh (Fig. 2 *B'*), which can diffuse at much longer distances compared with normal Hh (56). With cholesterol-free Hh, we observed the formation of ectopic boundaries within the segment. Studies show that groove formation requires the presence of an interface between groove cells and nongroove cells (19). Groove cells are marked by the expression of Odd. So we propose that Hh overexpression in the dorsal epidermis induces groove fate to all cells, and the absence of groove and nongroove cell interface leads to the loss of grooves at segment boundaries during the late stage of embryogenesis. However, as the contractile forces in the segment still exist, the movement of the T2 segment continues independently of the groove formation. This movement is inhibited by the cells located at the T1-T2 segment boundary, which must move inward to allow the movement of the T2

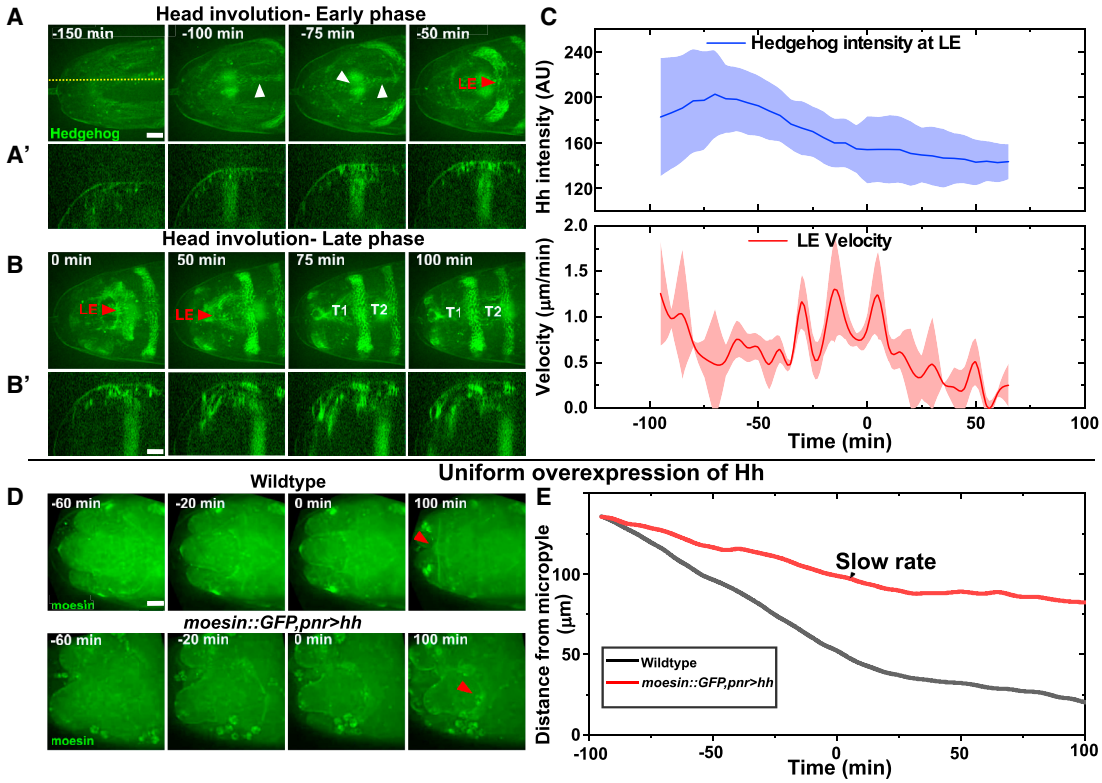

FIGURE 4 Head involution and epidermal spreading occur during spatiotemporal pulses of Hh signaling. (*A*) Time-lapse images showing the Hh pattern during the epithelial spreading. Hh is expressed in a stripe of cells in the head tissue during the initial stages of spreading (*white arrow*). Cross-sectional view shows that the Hh expression is initiated in the head tissue (*white arrow*) as the head involution begins to start (n = 4 embryos). Moreover, Hh is clearly expressed posterior to the LE (*red arrow*) during the initial stages of spreading (n = 4 embryos). Here, t = 0 is the time when the LE is ~50 microns from the micropyle. (*B*) Time-lapse images showing the Hh pattern during the later stages of head involution. Hh activity at the LE gradually declines as the spreading progresses (*red arrow*). (*C*) Graph quantifying the Hh intensity at the leading edge and velocity of the LE. The Hh intensity at the LE drops as time progresses. Similarly, we observe a decrease in the velocity of the LE as time progresses (n = 3). (*D*) Time-lapse images comparing the epithelial spreading of a *Drosophila* embryo expressing *pnr-Gal4, moesin: GFP* (wild-type) and *pnr-Gal4, moesin: GFP* × *UAS-hh*. Uniform overexpression of Hh impairs the spreading, and head involution does not complete. (*E*) Graphs comparing the leading-edge progression with respect to time for wild-type and *UAS-hh*. The progress of the LE is very slow when compared to wild-type. All scale bars represent 25 microns. To see the figure in color, go online.

segment. As the cells located at the T1-T2 segment boundary could not move inward, forces from the T2 segment exerts a compressive force within the segment. Because of the compressive forces, the cells start forming boundaries within the segment (Video S6). Together, these results suggest that the groove formation is required and essential for initiating the fold formation at the T1-T2 and T2-T3 segment boundaries. Without apical constriction, the forces within the T2 segment are not enough for generating folds. In summary, these results suggest that the overexpression of Hh in the dorsal epidermis during the late stage of embryogenesis leads to several morphogenetic defects, varying from incomplete head involution to incomplete fold formation.

Defects in cell shapes accompanies folding phenotypes when Hh is overexpressed

Previous investigations reported a gradient in contractile forces across each segment (17) responsible for the movement of the segments. Uniform overexpression of Hh homogenizes this gradient and thus disrupts the forces necessary for the positioning of the segments. Thus, we asked whether the presence of these gradients drives the folding process. We measured the cell shapes in the T2 segment as it begins to fold as an indicator of the balance of cell tension. As reported earlier (17), cells are more elongated in the D-V direction at the anterior end of the T2 segment and more circular at the posterior end (Fig. 5 *A*; Fig. S2 *A*). Additionally, we observed that the apical widths along the anterior-posterior axis are lower at the anterior of the segment when compared to the posterior (Fig. S2 *A*). In addition to previous observations (17), we observed that there exists a gradient in the cell area across the T2 segment. Also, we measured the shapes for the cells outside the folds across the segment during the folding process. We observed the cell shape profile across the segment remained similar during the fold formation (Fig. 5, *A* and *B*).

Next, we analyzed the cell shapes for embryos with uniform overexpression of Hh. We observed that the cells located at the anterior end of the T2 segment were more tightly packed

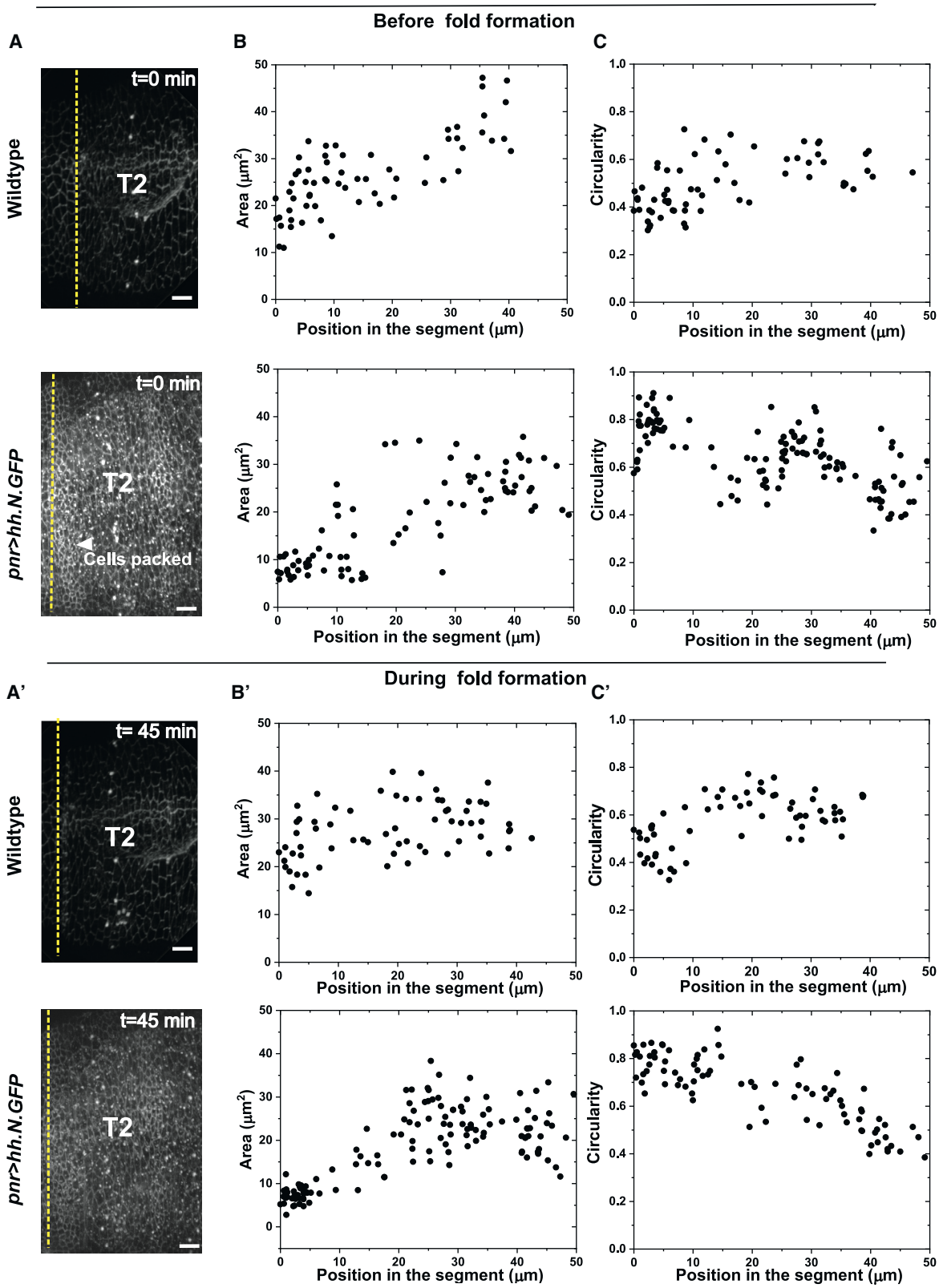

FIGURE 5 Comparison of cell shapes before and during folding. (*A*) Figure showing the T2 segment before the fold formation in both wild-type and Hh overexpression embryos. (*B*) A gradient in the cell areas across the segment for both wild-type and Hh overexpression embryos is observed. (*C*) Similar to past observations, cell circularity was patterned during folding in wild-type embryos. However, the cells have higher circularity at the anterior end of the T2 segment for Hh overexpression embryos. (*A'*, *B'*, and *C'*) Figure comparing the shapes of cells outside the folds and during the fold formation across the T2 segment. The cell shape profile did not change qualitatively during the folding process. All scale bars represent 10 microns. To see the figure in color, go online.

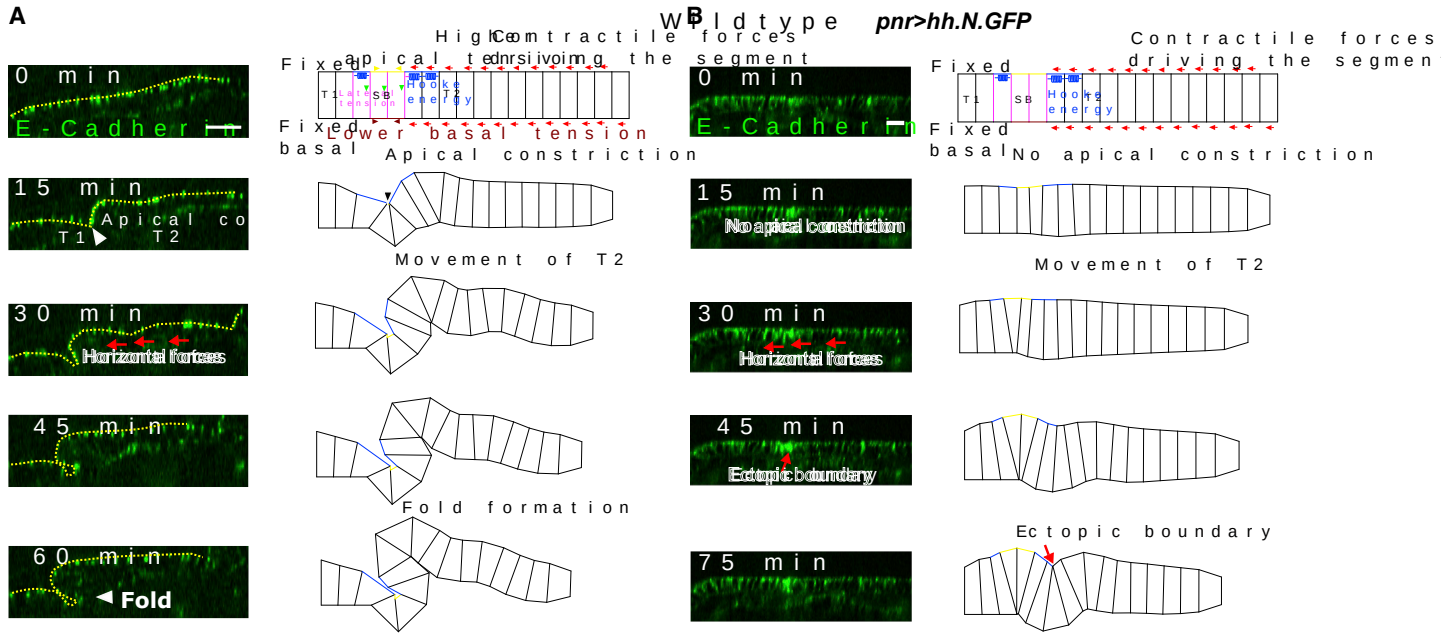

FIGURE 6 Computational model shows that apical constriction is necessary for fold formation at the segment boundaries. (*A*) Simulation showing the fold formation in which both apical constriction and contractile forces are present. Fold forms due to combination of apical constriction and contractile forces driving the movement of T2 segment. (*B*) Computational model simulating the cross section of the T1-T2 segment for a Hh overexpression embryo. In the model, forces driving the apical constriction are absent, and the contractile forces driving the segment movement still exist. As the T2 segment moves, the cells near the segment boundary experience a compressive force, resulting in a mild constriction, leading to an ectopic boundary. All scale bars represent 10 microns. To see the figure in color, go online.

and round for two to three rows of cells (Fig. 5, *A* and *B*). Interestingly, we did not observe homogenization of cell circularity across the segments. Cells were more circular at the anterior end of the T2 segment for three rows of cells when compared to the posterior end. In addition, the cells located at the anterior end of the T2 segment were not elongated along the D-V axis (Fig. S2 *B*). The cells located at the anterior end of the T2 segment are groove founder cells (21) and participate in the groove formation. In wild-type embryos, the groove founder cells are elongated along the D-V axis and less circular (Fig. S2 *A*). In Hh overexpression embryos, these cells are not elongated and are more round, which indicates higher apical contractility. Moreover, we observed that the cells located at the anterior end of the T2 segment showed increased levels of E-cadherin intensities, indicating strong cell-cell contacts (Fig. S3). Together, these results suggest that Hh overexpression leads to an increase in cells reducing their apices at the anterior end of the T2 segment but fail to form grooves because of the absence of an interface between nongroove and groove cells (19).

Groove formation and contractile forces contribute to epithelial folding

To formally test the mechanism regarding fold formation at the T1/T2 boundary, we formulated a mechanical model representing the cross section of the epithelium. Local active forces are incorporated by specifying the relative apical, basal, and lateral tension along cell boundaries. Groove formation was initiated by increasing the lateral and apical tension in the cells at the T1-T2 segment boundary. Simultaneously, the horizontal forces are exerted on the T2 segment cells. By incorporating both mechanisms (apical constriction and tissue-level compression), we qualitatively reproduced the fold morphology that we observed in wild-type embryos (Fig. 6 *A*). Next, we removed the forces representing the contractile actomyosin rings forming between cell rows. When we removed the tissue-level forces, we observed normal apical constriction at the T1-T2 segment boundary. But we did not observe the movement of the T2 cells over the constricted cells. Next, we only applied the horizontal forces on the T2 segment cells and blocked the groove formation at the segment boundary (Fig. 6 *B*). As expected, cells at the segment boundary experienced the compressive force, resulting in a mild constriction as the tissue undergoes buckling because of compressive stress. However, the compressive force was unable to induce the observed fold morphology. Thus, the mechanical model confirms that the fold formation at the segment boundaries occurs because of a combined operation of forces from groove formation and contractile actomyosin cables within the segment (Video S7).

DISCUSSION

The epithelial folds that form during the later stages of embryogenesis partition the epithelia into different segments.

Here, we identified that both apical constriction and forces within the segment contribute to fold formation. Further, we identified that Hh signaling is both spatially and temporally patterned during this complex process. Hh signaling is a conserved mode of intercellular communication necessary for embryogenesis (22). Hh proteins travel over multiple cell rows within a developing tissue to regulate diverse cellular responses in a concentration- and time-dependent manner (57,58). Dysregulation of the production of these Hh ligands during development produces debilitating congenital disorders (59). Several questions regarding Hh, such as how the developmental outcomes depend on the strength and duration of Hh signaling and how it regulates cytoskeletal dynamics, remain poorly understood (60–63). For example, Corrigall et al. (29) showed that the level of tissue invagination in *Drosophila* epithelia varies with the exposure time of Hh. A recent study shows that the activation of Hh in the dorsal epidermis of a *Drosophila* embryo slows down the epithelial spreading and disrupts segment positioning by disturbing the spatial patterning of the contractile activity in the segments (17). However, open questions remain regarding the precise molecular mechanisms through which Hh regulates the cytoskeletal activity during head involution and segment positioning. Further investigations into this mechanism will help us in understanding how coordinated cell shape changes are linked to global patterning information during epithelial morphogenesis.

Additionally, we observed that the Hh signaling appears as a stripe along the dorsal midline of the cells in the head tissue, at the beginning of head involution (Fig. S4). Further study is needed to investigate the roles of these Hh pulses in the head tissue. Also, the temporal regulators of Hh signaling in the head tissue is unknown. One possibility is that these Hh pulses might initiate the head involution process in the head tissue. Further, we identified that Hh signaling dynamics at the LE correlates with the relative velocity profile. Overexpression of Hh arrested the movement of the LE, resulting in head involution defects. Additional future work is needed to investigate the correlation between the pulse of the Hh signal at the LE and the movement of the LE. We identified that fold formation occurs at the segment boundaries after completion of head involution, and Hh is spatiotemporally patterned during this process. Disruption of this pattern by uniform overexpression leads to the formation of ectopic boundaries. Previous studies have shown that Hh induces groove cell fate (21) and is responsible for groove formation during stages 13–15 of embryogenesis (19). Here, we show that patterned Hh signal is also necessary for the formation of intersegmental grooves in the dorsal epidermis during later stages of embryogenesis. These grooves initiate the fold formation at the T1-T2 and T2-T3 segment boundaries. Czerniak et al. (17) showed that grooves are less indented in the Hh overexpression embryos when compared to the wild-type. Our study shows that Hh overexpression in the dorsal epidermis inhibits the groove formation. Forces behind the groove invagination can be majorly due to global tissue rearrangement or autonomous action of the epidermal cells located at the segment boundaries (21,35). Here, we identified that the movement of the T2 segment was unable to rescue the loss of groove observed with Hh overexpression embryos. Instead, it exerted compressive stress on the cells, leading to the formation of ectopic boundaries within the segment. Our study identifies a specific mechanism in which forces from both the cellular and tissue level operate in parallel to drive the fold formation at the segment boundaries. The computational model recapitulates the fold morphology when forces are incorporated at both the cellular and tissue level. Future studies are needed to investigate the interplay between the local and global forces and quantitatively analyze their respective contributions in driving the fold formation at the segment boundaries. In sum, epithelial folding in the late stages of embryogenesis depends on the joint action of multiple mechanistic "folding" modules.

SUPPORTING MATERIAL

Supporting material can be found online at https://doi.org/10.1016/j.bpj.2021.08.028.

AUTHOR CONTRIBUTIONS

V.V. performed the experiments and simulations. V.V. and J.Z. performed the analysis and wrote the manuscript. J.Z. supervised the project.

ACKNOWLEDGMENTS

Authors in this project are grateful to Optical Microscopy Core and Notre Dame Imaging Center for the light-sheet microscopy. The authors also thank the members of Zartman laboratory for their valuable feedback.

The work was supported in part by National Science Foundation Chemical, Bioengineering, Environmental, and Transport Systems 1553826, National Science Foundation-Major Research Instrumentation Program 1919832, and National Institutes of Health grant R35GM124935.

REFERENCES

1. Zartman, J. J., and S. Y. Shvartsman. 2010. Unit operations of tissue development: epithelial folding. *Annu. Rev. Chem. Biomol. Eng.* 1:231–246.
2. Gilmour, D., M. Rembold, and M. Leptin. 2017. From morphogen to morphogenesis and back. *Nature.* 541:311–320.
3. Tozluoğlu, M., and Y. Mao. 2020. On folding morphogenesis, a mechanical problem. *Philos. Trans. R. Soc. Lond. B Biol. Sci.* 375:20190564.
4. Pearl, E. J., J. Li, and J. B. A. Green. 2017. Cellular systems for epithelial invagination. *Philos. Trans. R. Soc. Lond. B Biol. Sci.* 372:20150526.
5. Zulueta-Coarasa, T., and R. Fernandez-Gonzalez. 2017. Tension (re) builds: biophysical mechanisms of embryonic wound repair. *Mech. Dev.* 144:43–52.
6. Belacortu, Y., and N. Paricio. 2011. Drosophila as a model of wound healing and tissue regeneration in vertebrates. *Dev. Dyn.* 240:2379–2404.

7. Zhang, W., K. Kai, …, L. Qin. 2013. A brief review of the biophysical hallmarks of metastatic cancer cells. *Cancer Hallm.* 1:59–66.
8. Vijayraghavan, D. S., and L. A. Davidson. 2017. Mechanics of neurulation: from classical to current perspectives on the physical mechanics that shape, fold, and form the neural tube. *Birth Defects Res.* 109:153–168.
9. Hilton, W. A. 1902. The morphology and development of intestinal folds and Villi in vertibrates. *Am. J. Anat.* 1:459–505.
10. Sumigray, K. D., M. Terwilliger, and T. Lechler. 2018. Morphogenesis and compartmentalization of the intestinal crypt. *Dev. Cell.* 45:183–197.e5.
11. Polyakov, O., B. He, …, E. Wieschaus. 2014. Passive mechanical forces control cell-shape change during Drosophila ventral furrow formation. *Biophys. J.* 107:998–1010.
12. Martin, A. C., and B. Goldstein. 2014. Apical constriction: themes and variations on a cellular mechanism driving morphogenesis. *Development.* 141:1987–1998.
13. Wang, Y.-C. 2021. The origin and the mechanism of mechanical polarity during epithelial folding. *Semin. Cell Dev. Biol.* S4084–9521:00136, 1.
14. Wang, Y.-C., Z. Khan, …, E. F. Wieschaus. 2012. Differential positioning of adherens junctions is associated with initiation of epithelial folding. *Nature.* 484:390–393.
15. Sherrard, K., F. Robin, …, E. Munro. 2010. Sequential activation of apical and basolateral contractility drives ascidian endoderm invagination. *Curr. Biol.* 20:1499–1510.
16. Chung, S., S. Kim, and D. J. Andrew. 2017. Uncoupling apical constriction from tissue invagination. *eLife.* 6:e22235.
17. Czerniak, N. D., K. Dierkes, …, J. Solon. 2016. Patterned contractile forces promote epidermal spreading and regulate segment positioning during Drosophila head involution. *Curr. Biol.* 26:1895–1901.
18. VanHook, A., and A. Letsou. 2008. Head involution in Drosophila: genetic and morphogenetic connections to dorsal closure. *Dev. Dyn.* 237:28–38.
19. Mulinari, S., and U. Häcker. 2009. Hedgehog, but not Odd skipped, induces segmental grooves in the Drosophila epidermis. *Development.* 136:3875–3880.
20. Urbano, J. M., H. W. Naylor, …, B. Sanson. 2018. Suppression of epithelial folding at actomyosin-enriched compartment boundaries downstream of Wingless signalling in *Drosophila*. *Development.* 145:dev155325.
21. Larsen, C. W., E. Hirst, …, J.-P. Vincent. 2003. Segment boundary formation in Drosophila embryos. *Development.* 130:5625–5635.
22. Varjosalo, M., and J. Taipale. 2008. Hedgehog: functions and mechanisms. *Genes Dev.* 22:2454–2472.
23. Jia, Y., Y. Wang, and J. Xie. 2015. The Hedgehog pathway: role in cell differentiation, polarity and proliferation. *Arch. Toxicol.* 89:179–191.
24. Lu, J., D. Wang, and J. Shen. 2017. Hedgehog signalling is required for cell survival in Drosophila wing pouch cells. *Sci. Rep.* 7:11317.
25. Bale, A. E. 2002. Hedgehog signaling and human disease. *Annu. Rev. Genomics Hum. Genet.* 3:47–65.
26. Gupta, S., N. Takebe, and P. Lorusso. 2010. Targeting the Hedgehog pathway in cancer. *Ther. Adv. Med. Oncol.* 2:237–250.
27. Pak, E., and R. A. Segal. 2016. Hedgehog signal transduction: key players, oncogenic drivers, and cancer therapy. *Dev. Cell.* 38:333–344.
28. Callejo, A., A. Bilioni, …, I. Guerrero. 2011. Dispatched mediates Hedgehog basolateral release to form the long-range morphogenetic gradient in the Drosophila wing disk epithelium. *Proc. Natl. Acad. Sci. USA.* 108:12591–12598.
29. Corrigall, D., R. F. Walther, …, F. Pichaud. 2007. Hedgehog signaling is a principal inducer of Myosin-II-driven cell ingression in Drosophila epithelia. *Dev. Cell.* 13:730–742.
30. Biehs, B., K. Kechris, S. Liu, and T. B. Kornberg. 2010. Hedgehog targets in the Drosophila embryo and the mechanisms that generate tissue-specific outputs of Hedgehog signaling. *Development.* 137:3887–3898.
31. Jia, J., C. Tong, and J. Jiang. 2003. Smoothened transduces Hedgehog signal by physically interacting with Costal2/Fused complex through its C-terminal tail. *Genes & development.* 17:2709–2720.
32. Méthot, N., and K. Basler. 1999. Hedgehog controls limb development by regulating the activities of distinct transcriptional activator and repressor forms of Cubitus interruptus. *Cell.* 96:819–831.
33. Aza-Blanc, P., F. A. Ramírez-Weber, M. P. Laget, C. Schwartz, and T. B. Kornberg. 1997. Proteolysis that is inhibited by hedgehog targets Cubitus interruptus protein to the nucleus and converts it to a repressor. *Cell.* 89:1043–1053.
34. Lawrence, P. A., and G. Struhl. 1996. Morphogens, compartments, and pattern: lessons from drosophila? *Cell.* 85:951–961.
35. Mulinari, S., M. P. Barmchi, and U. Häcker. 2008. DRhoGEF2 and diaphanous regulate contractile force during segmental groove morphogenesis in the Drosophila embryo. *Mol. Biol. Cell.* 19:1883–1892.
36. Kursawe, J., P. A. Brodskiy, …, A. G. Fletcher. 2015. Capabilities and limitations of tissue size control through passive mechanical forces. *PLoS Comput. Biol.* 11:e1004679.
37. Brodland, G. W. 2015. How computational models can help unlock biological systems. *Semin. Cell Dev. Biol.* 47–48:62–73.
38. Nematbakhsh, A., W. Sun, …, M. Alber. 2017. Multi-scale computational study of the mechanical regulation of cell mitotic rounding in epithelia. *PLoS Comput. Biol.* 13:e1005533.
39. Nematbakhsh, A., M. Levis, …, M. Alber. 2020. Epithelial organ shape is generated by patterned actomyosin contractility and maintained by the extracellular matrix. *PLoS Comput. Biol.* 16:e1008105.
40. Tetley, R. J., G. B. Blanchard, …, B. Sanson. 2016. Unipolar distributions of junctional Myosin II identify cell stripe boundaries that drive cell intercalation throughout Drosophila axis extension. *eLife.* 5:e12094.
41. Tetley, R. J., M. F. Staddon, Y. Mao…, 2019. Tissue fluidity promotes epithelial wound healing. *Nat. Phys.* 15:1195–1203.
42. Hartman, T. R., T. I. Strochlic, …, A. M. O'Reilly. 2013. Diet controls Drosophila follicle stem cell proliferation via Hedgehog sequestration and release. *J. Cell Biol.* 201:741–757.
43. Chen, W., H. Huang, …, T. B. Kornberg. 2017. Essential basal cytonemes take up Hedgehog in the *Drosophila* wing imaginal disc. *Development.* 144:3134–3144.
44. Duda, M., N. J. Kirkland, …, Y. Mao. 2019. Polarization of myosin II refines tissue material properties to buffer mechanical stress. *Dev. Cell.* 48:245–260.e7.
45. Schindelin, J., I. Arganda-Carreras, …, A. Cardona. 2012. Fiji: an open-source platform for biological-image analysis. *Nat. Methods.* 9:676–682.
46. Weigert, M., U. Schmidt, …, E. W. Myers. 2018. Content-aware image restoration: pushing the limits of fluorescence microscopy. *Nat. Methods.* 15:1090–1097.
47. Aigouy, B., C. Cortes, …, B. Prud'Homme. 2020. EPySeg: a coding-free solution for automated segmentation of epithelia using deep learning. *Development.* 147:dev194589.
48. Brakke, K. A. 1992. The surface evolver. *Exp. Math.* 1:141–165.
49. Štorgel, N., M. Krajnc, …, P. Ziherl. 2016. Quantitative morphology of epithelial folds. *Biophys. J.* 110:269–277.
50. Hočevar Brezavšček, A., M. Rauzi, …, P. Ziherl. 2012. A model of epithelial invagination driven by collective mechanics of identical cells. *Biophys. J.* 103:1069–1077.
51. Schaumann, E. N., M. F. Staddon, …, S. Banerjee. 2018. Force localization modes in dynamic epithelial colonies. *Mol. Biol. Cell.* 29:2835–2847.
52. Fletcher, A. G., F. Cooper, and R. E. Baker. 2017. Mechanocellular models of epithelial morphogenesis. *Philos. Trans. R. Soc. Lond. B Biol. Sci.* 372:20150519.
53. Hayes, P., and J. Solon. 2017. Drosophila dorsal closure: an orchestra of forces to zip shut the embryo. *Mech. Dev.* 144:2–10.

54. Peralta, X. G., Y. Toyama, …, G. S. Edwards. 2007. Upregulation of forces and morphogenic asymmetries in dorsal closure during Drosophila development. *Biophys. J.* 92:2583–2596.

55. Busson, D., and A.-M. Pret. 2007. GAL4/UAS targeted gene expression for studying Drosophila Hedgehog signaling. *Methods Mol. Biol.* 397:161–201.

56. Ducuing, A., B. Mollereau, …, S. Vincent. 2013. Absolute requirement of cholesterol binding for Hedgehog gradient formation in Drosophila. *Biol. Open.* 2:596–604.

57. Kiecker, C., A. Graham, and M. Logan. 2016. Differential cellular responses to Hedgehog signalling in vertebrates-what is the role of competence? *J. Dev. Biol.* 4:36.

58. Petrova, R., and A. L. Joyner. 2014. Roles for Hedgehog signaling in adult organ homeostasis and repair. *Development.* 141:3445–3457.

59. Nieuwenhuis, E., and C. C. Hui. 2005. Hedgehog signaling and congenital malformations. *Clin. Genet.* 67:193–208.

60. Harfe, B. D., P. J. Scherz, …, C. J. Tabin. 2004. Evidence for an expansion-based temporal Shh gradient in specifying vertebrate digit identities. *Cell.* 118:517–528.

61. Scherz, P. J., E. McGlinn, …, C. J. Tabin. 2007. Extended exposure to Sonic hedgehog is required for patterning the posterior digits of the vertebrate limb. *Dev. Biol.* 308:343–354.

62. Dessaud, E., L. L. Yang, …, J. Briscoe. 2007. Interpretation of the sonic hedgehog morphogen gradient by a temporal adaptation mechanism. *Nature.* 450:717–720.

63. Escudero, L. M., M. Bischoff, and M. Freeman. 2007. Myosin II regulates complex cellular arrangement and epithelial architecture in Drosophila. *Dev. Cell.* 13:717–729.